Self-reactivity of a calcined palygorskite-bearing marlstone for potential use as supplementary cementitious material

Victor Poussardin, Michael Paris, William Wilson, Arezki Tagnit-Hamou, Dimitri Deneele

Applied Clay Science 216 (2022) 106372

Contents lists available at ScienceDirect

Applied Clay Science

journal homepage: www.elsevier.com/locate/clay

Research paper

Self-reactivity of a calcined palygorskite-bearing marlstone for potential use as supplementary cementitious material

Victor Poussardin [a,b,c], Michael Paris [b], William Wilson [c], Arezki Tagnit-Hamou [c], Dimitri Deneele [a,b,*]

[a] GERS-GIE, Univ Gustave Eiffel, IFSTTAR, F-44344 Bouguenais, France
[b] Université de Nantes, CNRS, Institut des Matériaux Jean Rouxel, IMN, F-44000 Nantes, France
[c] Université de Sherbrooke, Sherbrooke, QC, Canada

ARTICLE INFO

Keywords:
Palygorskite
Marlstone
Pozzolanic activity
MAS NMR
Calcined clay

ABSTRACT

This article focuses on the study of the self-reactivity of a 800 °C calcined palygorskite-bearing marlstone which is a complex multi-phase system (including CaO and MgO) whose reactivity in water must be studied before being used as Supplementary Cementitious Material (SCM). The sample was hydrated (w/s = 0.8) for 7, 14, 28 and 180 days and then investigated using X-ray diffraction (XRD), Solid State Nuclear Magnetic Resonance (MAS NMR), and Scanning Electron Microscope (SEM). Crossing the results of XRD and MAS NMR analyses (in particular the phase quantification by spectral integration of ^{29}Si MAS NMR spectra) have revealed the reactivity of the calcined clay phases with the portlandite which leads to the formation of C-(A)-S-H. It also highlighted the reactivity of C_2S (neoformed during calcination) within 7 days of hydration. Hydration of this sample showed high self-reactivity (mostly pozzolanic) making it a promising sample for use as SCM.

1. Introduction

The cement demand has been increasing over the past few decades (Amran et al., 2020), mainly as a result of the population and economic growth (Mikulčić et al., 2016). Countries and especially developing countries are rapidly building up industrial and transport infrastructures to cope with their economic development. It is estimated that the cement industry is responsible for 5 to 8% of the total anthropogenic CO_2 emissions (Huntzinger and Eatmon, 2009) and 95% of this CO_2 is emitted during the manufacturing process (Cancio Díaz et al., 2017). In recent years, environmental legislation has become more drastic in order to reduce the amount of CO_2 emission of cement production, and the cement industries have turned to research and development of new innovations that can reduce the environmental footprint of cement.

The use of Supplementary Cementitious Materials (SCMs) as a substitute for clinker is one of the emerging technology that could significantly reduce the environmental footprint of cement manufacturing. Among the widely used SCMs there are industrial wastes which have hydraulic properties, and in the presence of water react to form hydrates responsible for setting and hardening (e.g. blast furnace slag (Behim et al., 2002; Yazıcı et al., 2010) and fly ash (Yao et al., 2015; Hu et al., 2019)). However, blast furnace slag resources are not abundant enough to be used on a sustainable basis and the energetic transition rightly limits the availability of fly ash resources from coal combustion (Scrivener et al., 2018).

For several years now, the use of calcined clays as SCMs has been increasing. Indeed, the reserves of clays with potential for calcination are considerable and globally homogeneously distributed (Scrivener et al., 2018), making it a first choice resource for use as a SCM. Numerous studies have been carried out in recent years on the reactivity of different types of calcined clays in cementitious system and metakaolin resulting from the calcination of kaolin appeared the most promising (Alujas et al., 2015; Almenares et al., 2017; El-Diadamony et al., 2018; Zhao and Khoshnazar, 2020), whereas the calcined smectites (Brown et al., 1987; Garg and Skibsted, 2014; Kaminskas et al., 2020) and illites (Fernandez et al., 2011; Taylor-Lange et al., 2014; Garg and Skibsted, 2016) show much less encouraging results. However, it is important to remember that clays are not limited to the kaolinite, smectite and illite families. Many mining wastes contain clay phases, particularly unconventional clays whose use as SCM has never been studied.

The present study takes place in a project targeting the valorization

* Corresponding author at: GERS-GIE, Univ Gustave Eiffel, IFSTTAR, F-44344 Bouguenais, France.
E-mail address: dimitri.deneele@univ-eiffel.fr (D. Deneele).

https://doi.org/10.1016/j.clay.2021.106372
Received 8 September 2021; Received in revised form 2 December 2021; Accepted 7 December 2021
Available online 13 December 2021

of secondary resources (mining waste) as SCM. The thermal reactivity of the sample has already been studied and a temperature of 800 °C has been determined as an optimum (Poussardin et al., 2020). Upon calcination, the initial composition of this natural sample leads to the formation of reactive phases such as calcined clays, lime, periclase and C_2S. This composition is therefore very different from that of the classical SCMs currently in use. The presence of lime and periclase can be problematic factor for the use of this sample as SCM and should be considered. It is a very complex system whose reactivity cannot be directly studied in a cementitious system as usual.

This paper focuses on the reactivity of a mining waste from a phosphate mine initially composed of 17% of palygorskite and 16% of smectite (Poussardin et al., 2020). The particularity of this material is that it contains palygorskite - a particular TOT clay whose pozzolanic reactivity after calcination has not yet been studied – as well as reactive free lime and C_2S neoformed (Poussardin et al., 2020).

The first step is to study its self-reactivity in presence of water in order to understand the contribution of each phases composing it, their evolution and the possible presence of synergies. In order to be able to accurately characterize the self-reactivity of this sample, different characterization techniques have been used, such as X-ray Diffraction, Nuclear Magnetic Resonance and Scanning Electron Microscopy.

2. Materials and experimental methods

2.1. Materials

The material used is a natural marlstone considered as waste by the mining industry which is looking for new ways of recovery. Table 1 shows the chemical analysis of the raw sample carried out by X-Ray Fluorescence (XRF), the proportions are given in oxides (expressed in weight %).

The physicochemical properties and the optimal calcination of this material have been investigated in a previous article (Poussardin et al., 2020).

The raw material is composed of a mixture of dolomite (54 wt%), palygorskite (17 wt%), Ca-smectite (16 wt%), quartz (8 wt%), hydroxylapatite (3 wt%), and biotite (2 wt%). A calcination temperature of 800 °C has been selected to allow an important dehydroxylation of the clay phases while avoiding recrystallization phenomena. During the calcination process, different reactive phases were formed, such as: lime (19 wt%), periclase (17 wt%) and C_2S (4 wt%)".

2.2. Materials hydration

The raw natural sample has a high proportion of dolomite ($CaMg(CO_3)_2$) which, during calcination, led to the formation of lime (CaO). Therefore this sample is not suitable for the classical pozzolanic activity tests such as the R^3 screening (Avet et al., 2016), Frattini test or saturated lime test (Tironi et al., 2013) since they all assume that the test sample does not contain free calcium. It was therefore decided to characterize the reactivity of the sample by a different approach: the reaction of the sample in water. During the hydration of this calcined material, the lime is hydrated into portlandite which becomes available to react pozzolanically with the calcined clay phases (palygorskite, smectite and biotite). In addition, hydration allows testing whether the C_2S neoformed during calcination is reactive.

One gram of marlstone calcined at 800 °C was manually mixed with water according to the selected water-to-solid ratios (w/s = 0.8, 1, 2 and 4) until a homogeneous paste was obtained. The vials where then closed and left to react during 7, 14, 28 and 180 days at room temperature in sealed conditions (without atmosphere control). At the end of each curing time the samples were freeze-dried for 48 h in order to stop hydration. Within 2 days, the dry samples were crushed and analyzed by XRD, MAS NMR, and SEM. Since the results are similar across all w/s ratios tested with respect to all ages, only the results for w/s = 0.8 are presented in this article.

2.3. Phases analyses

2.3.1. X-ray diffraction

The diffractograms were acquired on a Bruker D8 diffractometer based on a Bragg-Brentano geometry. The X-ray source consists of a copper anode tube (40 kV/40 mA) that emits Cu Kα radiation. The X-ray diffractograms of disoriented powdered sample were acquired between 5° and 60° 2θ with a step size of 0.017° 2θ and a measurement time of 1 s per step. The identification of XRD peaks was done with the PROFEX software database (BGMN PROGRAM) (Doebelin and Kleeberg, 2015).

2.3.2. Nuclear magnetic resonance

The ^{27}Al MAS NMR spectra were acquired on a Bruker Avance III 500 MHz spectrometer using a 2.5 mm MAS probe. The excitation pulse length used was π/13 for a radio frequency field of 11 kHz. The repetition time was 1 s and the MAS frequency was 30 kHz.

The ^{29}Si MAS NMR spectra were acquired on a Bruker NEO 300 MHz spectrometer using a 7 mm MAS probe. A π/2 excitation pulse length was used, and the MAS frequency was 5 kHz. After several tests of different repetition times the choice was made to use a time of 10s in order to ensure quantitative results except for quartz. However, it has no consequences as quartz is non-reactive.

^1H decoupling was performed during all the acquisitions. ^{27}Al spectra were referenced against an aqueous solution of $Al(NO_3)_3$ and ^{29}Si spectra against TMS (Tetramethylsilane). The spectral decompositions have been done using the dmfit software (Massiot et al., 2002).

2.3.3. Scanning electron microscope

The morphological changes during the hydration were examined by scanning electron microscopy (SEM). The analysis was carried out using a Hitachi SU5000 microscope. The samples were subjected to a platine coating before SEM observations.

3. Results and discussion

3.1. X-ray diffraction analysis

Fig. 1 displays the evolution of the diffractograms of the marlstone (labelled AC) calcined at 800 °C (AC-800) and hydrated during 7 days (AC-800-7d), 14 days (AC-800-14d), 28 days (AC-800-28d), and 180 days (AC-800-180d).

The XRD pattern of the sample calcined at 800 °C (AC-800) displays different peaks. The peaks associated with dehydrated smectite (Sm dehy) and biotite (Bio) are still detectable. In contrast, the peaks of palygorskite are no longer observable after the 800 °C thermal treatment (Poussardin et al., 2020). There are also peaks from quartz (Qz), lime (Li), periclase (Pe), hydroxylapatite (Hy) and C_2S.

Above 7 days of hydration (AC-800-7d) there is a significant decrease in the intensity of the peaks associated with lime and periclase. This decrease is correlated with the appearance of new peaks corresponding to portlandite (Po), hydrotalcite (Ht), brucite (Br) and calcite (C). The

Table 1
Chemical analysis of the raw material.

Oxide	FeO	CaO	SiO_2	Al_2O_3	K_2O	TiO_2	Na_2O	V_2O_5	P_2O_5	MgO	LOI (1000 °C)
wt%	1.99	19.83	33.3	8.94	1.24	0.34	0.32	0.16	1.49	9.91	35.0

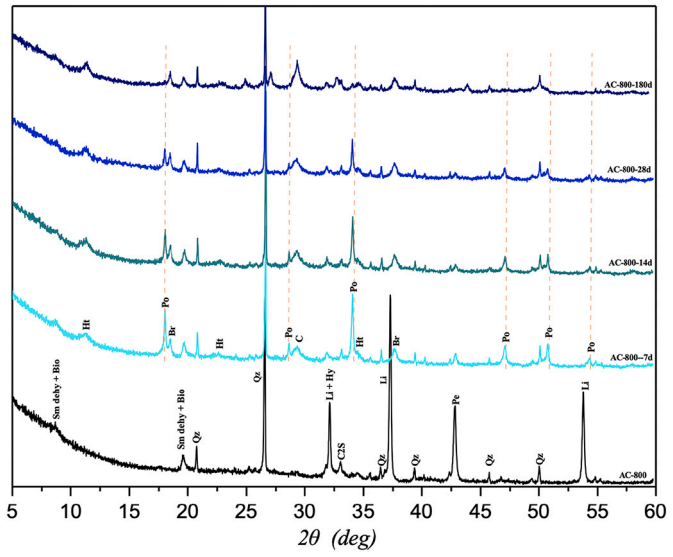

Fig. 1. Evolution of the diffractogram of the marlstone calcined at 800 °C and hydrated for 7, 14, 28 and 180 days, Sm = smectite; Bio = biotite; Ht = hydrotalcite; Po = portlandite; C = calcite; Qz = quartz; Hy = hydroxylapatite; Br = brucite; Li = lime; Pe = periclase; C_2S = dicalcium silicate.

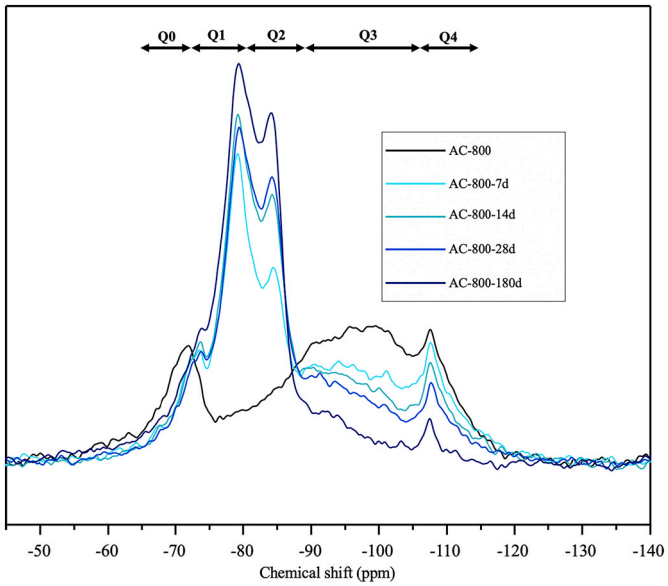

Fig. 2. Evolution of ^{29}Si MAS NMR spectra of the calcined marlstone as function of the hydration time.

formation of portlandite comes from the hydration of lime. The remaining signal of periclase in the hydrated sample could be explained by pockets of anhydrous periclase locked in a dense matrix of hydrates preventing water movement. The formation of calcite is due to the partial carbonation of the lime/portlandite (Van Balen and Van Gemert, 1994). The magnesium from periclase is incorporated into two new phases, brucite and hydrotalcite. However, the low intensity of the characteristic hydrotalcite peaks may suggests that most of the magnesium has been incorporated into brucite. ^{27}Al MAS NMR analysis will allow to characterize more precisely hydrotalcite formation during hydration.

The weak signals associated with the remaining clay phases (Sm dehy + bio) and C_2S remains present up to 180 days, demonstrating their non-reactivity.

As the hydration time is increasing, the main change observed is the decrease in the intensity of the peaks associated with portlandite until they are no longer detectable after 180 days of hydration. The remaining signal associated with periclase does not evolve. On the other hand, the intensity of the peak associated with calcite is increasing. The diffractogram evolution as a function of the hydration time allowed to highlight a decrease in the intensity of the peaks associated with portlandite, which reflects a portlandite consumption. However, it is difficult to attribute this consumption to the pozzolanic reaction because C-S-H cannot be characterized by XRD, it was therefore decided to use solid state NMR to characterize them.

3.2. *^{29}Si and ^{27}Al MAS NMR analysis*

Fig. 2 displays the evolution of the ^{29}Si MAS NMR spectra of the calcined marlstone hydrated for 7, 14, 28 and 180 days.

The AC-800 spectrum exhibits a resonance at −71 ppm which can be associated with monomeric Q^0 of C_2S (Skibsted et al., 1995) and a resonance at −108 ppm (Q^4) characteristic of quartz (Lippmaa et al., 1980). The broad signal of silicon in Q^3 configuration is composed of broad resonances of silicon in Q^3 configurations reflecting a distribution of their local environments and is characteristic of calcined palygorskite, and not fully calcined smectite and biotite (Poussardin et al., 2020). As it is not possible to distinguish the respective contributions of calcined palygorskite and incompletely calcined smectite and biotite in this signal, the term “calcined clay phases” has been used to designate them hereafter.

After 7 days of hydration, the intensities of the broad resonances associated with the Q^3 of the calcined clays decrease. The consumption of the calcined clay phases is correlated with the appearance of two new resonances at −78 and −85 ppm which correspond to silicon in Q^1 and Q^2 configuration, respectively (Magi et al., 1984). Silicon in Q^1 configuration can be associated with pairs of linked silicate tetrahedral (dimers) or with terminal silicate tetrahedral groups of C-S-H. Silicon in Q^2 configuration can be associated with silicate tetrahedral groups intermediates (Q^2-P) and/or bridging (Q^2-B) of C-S-H (Andersen et al., 2004).

The C_2S resonance at −71 ppm decreases considerably and leaves a resonance at −73 ppm which can either be associated with Q^0 of non-reactive C_2S or Q^1 of akermanite/gehlenite phase. The weak but non zero XRD signal of C_2S is remaining with increasing hydration time (see Fig. 1), this observation supports the hypothesis that the resonance at −71 ppm can be associated with Q^0 of non-reactive C_2S. On the other hand, the study of calcination has demonstrated recrystallization phenomena in the form of akermanite from 900 °C. This signal at −71 ppm, or a part of it, can therefore be associated with low-crystalline akermanite which is not yet observable by XRD at 800 °C. Finally, numerous studies have also demonstrated the formation of gehlenite during calcination of a marlstone (Shoval, 1988; Hughes et al., 2009; Verganelaki et al., n.d.), this −71 ppm signal could therefore also be associated with gehlenite.

At 14 days the consumption of the calcined clay phases progresses while the intensities of the Q^1 and Q^2 resonances characteristics of C-S-H are increasing. There is appearance of a new resonance at −81 ppm corresponding to Q^2(1Al) (Andersen et al., 2003) configuration in C-(A)-S-H (Gao et al., 2017). The apparition of Q^2(1Al) shows the incorporation of aluminium into the C-(A)-S-H structure.

The trend goes on with the hydration time until 180 days. The remaining resonance centered at −89 ppm corresponds to remaining calcined clay phases that did not react. The consumption of the calcined clay phases associated with the formation of C-(A)-S-H confirms the intrinsic pozzolanic reactivity of this calcined marlstone. It is important to note that the neoformed brucite could have reacted with SiO_2 to form M-S-H. However, the ^{29}Si MAS NMR signature of M-S-H is clearly different from the one observed which is characteristic of C-S-H (Bernard et al., 2017).

Fig. 3 gives the evolution of the relative proportions (from the

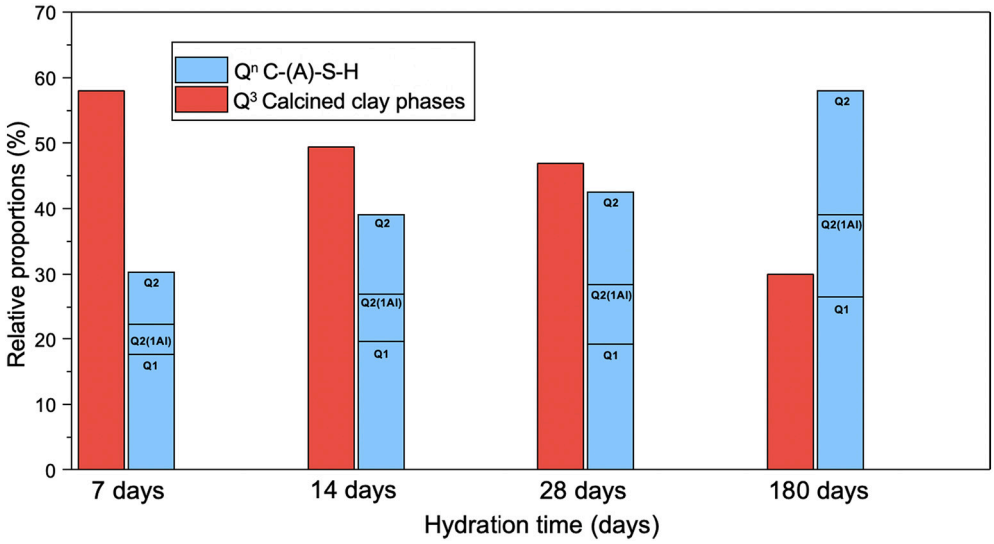

Fig. 3. Relative proportions of silicon-containing phases (from the perspective of silicon content) as function of the hydration time obtained from ^{29}Si NMR spectra.

perspective of silicon content) of Q^n associated with C-(A)-S-H and Q^3 associated with calcined clay phases as function of the hydration time. This quantification was done by spectral integration of the ^{29}Si NMR spectra (details in supporting information). As the signal of Q^4 associated with quartz is not quantitative and the relative proportion of Q^0/Q^1 associated with C_2S and/or akermanite/gehlenite is constant with the increase in hydration time it was decided to display the relative evolution between Q^3 associated with calcined clay phases and Q^n associated with C-(A)-S-H only.

Between 7 and 180 days the relative proportion of silicon in Q^3 configuration associated with the calcined clay phases decreases from 58% to 30%. In parallel, the relative proportion of silicon associated with the C-(A)-S-H ($Q^1 + Q^2(1Al) + Q^2$) increases from 30% to 58%.

The mean chain length (MCL) of aluminosilicate chains, the mean chain length of pure silicate units (MCL_{Si}) and the Al/Si ratio of the formed C-(A)-S-H can be calculated from ^{29}Si MAS NMR spectral deconvolutions by using the substituted general model (SGM) of Richardson and Groves (Richardson and Groves, 1993):

$$MCL = \frac{2\left[Q^1 + Q^2 + \left(\frac{3}{2}\right)Q^2\,(1Al)\right]}{Q^1}$$

$$MCL_{Si} = \frac{2\left[Q^1 + Q^2 + Q^2\,(1Al)\right]}{Q^1 + Q^2\,(1Al)}$$

$$\left(\frac{Al}{Si}\right) = \frac{\left(\frac{1}{2}\right)Q^2(1Al)}{Q^1 + Q^2 + Q^2(1Al)}$$

Table 2 displays the evolution of these 3 values as function of the hydration time.

The MCL, MCL_{Si} and Al/Si values are increasing with the hydration time between 7 and 14 days of hydration. After 14 days, the MCL_{Si} value does not evolve anymore. However, the MCL and Al/Si value still increase. This shows that the chains are lengthening by connecting silicate chains through AlO_4 units. Finally, the C-(A)-S-H structure remains stable after 28 days of hydration. It was not possible to find literature dealing with Al/Si, MCL and MCL_{Si} values in hydrated Metakaolin / CaO systems to undertake a comparative study. However, the Al/Si, MCL and MCL_{Si} values obtained are similar to those for C-(A)-S-H phases formed in hydrated white Portland cement-Metakaolin blends (Dai et al., 2014). This demonstrates that the C-(A)-S-H formed in this system are similar to those of Metakaolin-based blended cements. Knowing that Metakaolin blended cements are the most promising in terms of mechanical performance, this observation bodes well for the future use of this calcined marlstone as SCM.

Table 2
MCL, MCL_{Si} and Al/Si values as function of the hydration time calculated by using SGM.

Non-cross-linked C-(A)-S-H structure: substituted general model (SGM)			
Hydration time (days)	MCL	MCL_{Si}	Al/Si
7	3,69	2,72	0,076
14	4,37	2,90	0,094
28	4,91	2,99	0,108
180	4,86	2,97	0,109

It is important to note that the −89 ppm signal previously associated with remaining Q^3 of the calcined clay phases (Fig. 2) could also be associated with silicon in $Q^3(1Al)$ configuration related to cross-linking within the C-(A)-S-H structure (Gao et al., 2017). In this case, another model can be used to calculate MCL and Al/Si: a full cross-linked tobermorite model (Myers et al., 2013). Using this model, higher values were obtained for MCL and Al/Si (see supporting information). However, the evolution over the hydration time is similar to the one obtained from the SGM model. That clearly confirms that the C-(A)-S-H structure does not strongly depend on the hydration time.

Fig. 4 displays the evolution of the ^{27}Al MAS NMR spectra of the 800 °C calcined argillaceous carbonate hydrated for 7, 14, 28 and 180 days.

It was previously shown (Poussardin et al., 2020) that the AC-800 ^{27}Al MAS NMR spectrum is composed of 5 lines at 3.8, 6.5, 35, 61 and 69 ppm. The two former lines are associated with 6-fold aluminium whereas the 35 ppm line is associated with 5-fold aluminium. Finally, the 4-fold aluminium resonances at 61 and 69 ppm was attributed q4 to q3, respectively. 4-fold aluminium in q4 configuration and 5-fold aluminium are associated with the calcined clay phases. On the other hand, 4-fold aluminium in q3 configuration is close to what can be found in the gehlenite structure (Florian et al., 2012), which supports the hypothetical attribution of a part of the ^{29}Si NMR signal at −73 ppm to gehlenite-like Q^1 configuration.

After 7 days of hydration, an intense and narrow resonance appears at 10 ppm, which can be associated with aluminium found within the hydrotalcite previously detected by XRD (Prikhod'ko et al., 2001). The detection of this characteristic hydrotalcite NMR signal confirms the hypothesis that part of the magnesium from periclase is incorporated

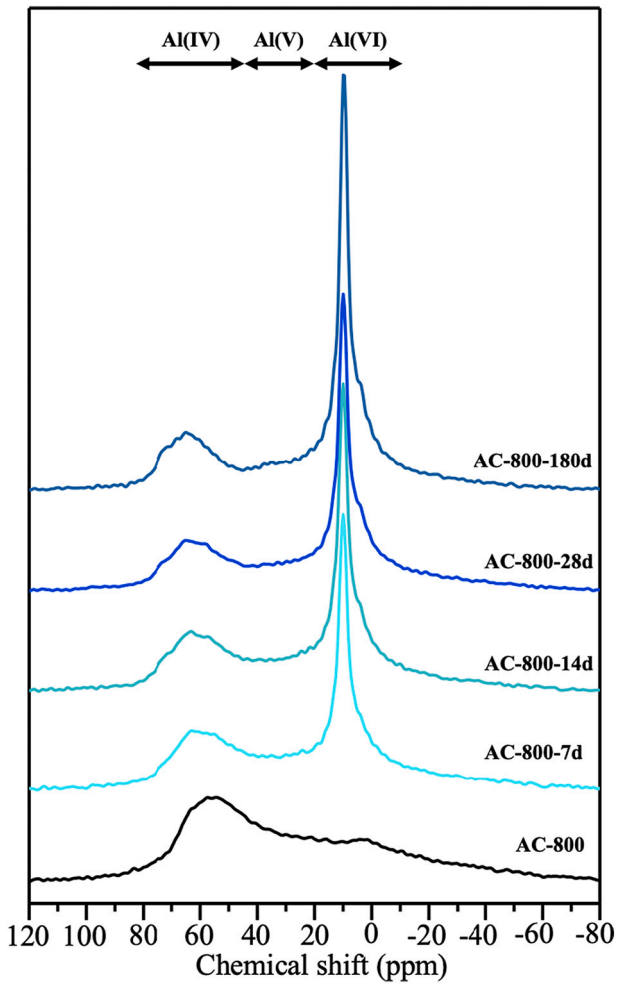

Fig. 4. Evolution of ^{27}Al MAS NMR spectra of the calcined marlstone as function of the hydration time.

directly into hydrotalcite in addition to brucite. This phenomenon has already been observed, notably during the hydration of alkali-activated blast-furnace slag (Haha et al., 2011; Cherki El Idrissi et al., 2018). Monocarboaluminates also resonate at 10 ppm in ^{27}Al MAS NMR, and their diffraction peaks at 11.6° 2θ and 23,5° 2θ overlap with those of hydrotalcite (Fig. 1) (Ipavec et al., 2011). Therefore, the possibility of formation of monocarboaluminate in addition to hydrotalcite cannot be excluded.

At 14 days of hydration there is appearance of a shoulder at 72 ppm which can be associated with 4-fold aluminium in q2 configuration (Pardal et al., 2012) characteristic of aluminium incorporated into C-(A)-S-H chains, confirming the ^{29}Si NMR results. The shoulder at 5 ppm suggests the presence of the third aluminate hydrate (TAH) formed at the surface of the C-(A)-S-H (Andersen et al., 2006) and/or can be explained by 6-fold aluminium within the structure of C-(A)-S-H (Kunhi Mohamed et al., 2020).

With the increase in hydration time there is a decrease in the intensity of the resonances previously associated with q4 Al(IV) and Al(V) thus reflecting the consumption of the calcined clay phases with time. On the other hand, the intensity of the resonance associated with q3 Al (IV) is not decreasing, suggesting that gehlenite potentially neoformed during calcination is not reactive. After 180 days it remains signal of q4 Al(IV) and Al(V) which correspond to the unreacted calcined clay phases whose Q^3 are still observable in ^{29}Si NMR (Fig. 2), due to the lack or portlandite.

3.3. Scanning electron microscope analysis

Fig. 5 displays the SEM images of powder of the marlstone calcined at 800 °C (Fig. 5A) and hydrated during 28 days (Fig. 5B, and C).

On the Fig. 5A it can be distinguished a covering which consists of needles and a veil that covers the entire surface of the sample. These types of morphology are respectively typical of calcined palygorskite and smectite (Boudriche et al., 2011). Even calcined, palygorskite and smectite morphology is conserved (Poussardin et al., 2020). After 28-day hydration, there is the apparition of a new coating (Fig. 5B and C) which is mainly composed of flocs. This morphology is characteristic of flocs-like C-(A)-S-H phases (Cizer et al., n.d.). This new C-(A)-S-H phase is covering/replacing the calcined clay phases supporting previous results suggesting C-(A)-S-H formation from pozzolanic reaction. It seems that reaction takes place at the interface between the calcined clay phases and the portlandite.

3.4. Potential use as supplementary cementitious material

As explained in the abstract, the objective of this study is not to obtain mechanical performance on cements incorporating the calcined material. The composition of this kind of material (marlstone) clearly differs from the classical SCMs currently in use. Consequently, it requires the use of an intermediate investigation step (self-reactivity under hydration) before mixing it with cement. The aim is to understand the evolution of the reactive phases (lime and periclase) neoformed during calcination and to characterize the pozzolanic reactivity of the calcined clay phases (palygorskite, smectite and biotite).

ASTM C618 standard states that a calcined clay is suitable for use as SCM if the sum of SiO_2, Al_2O_3 and Fe_2O_3 composing it is greater than or equal to 70% of the total oxide content. The 800 °C calcined marlstone studied in this article has a CaO content of 19.5% and a MgO content of 17% (Poussardin et al., 2020), therefore the sum SiO_2, Al_2O_3 and Fe_2O_3 composing it is lower than 70% of its total oxide content and it does not meet the recommendations given by this standard.

The problem of MgO comes from its hydration into $Mg(OH)_2$ which leads to a potential swelling phenomenon. As the formation of $Mg(OH)_2$ has slow kinetics compared to the hydration of the anhydrous phases of the clinker, a post-hardening swelling can occur and lead to the formation of cracks and therefore loss of resistance (Cherney and Hooton, 1987). XRD results reveal $Mg(OH)_2$ formation during hydration. On the other hand, XRD and ^{27}Al MAS NMR showed the formation of hydrotalcite after 7d of hydration. It thus appears that magnesium from MgO is found incorporated into both brucite and hydrotalcite and there is no swelling phenomenon related to the formation of hydrotalcite in the existing literature.

Free lime (CaO) content in cement has to be controlled in order to avoid undesirable effects such as reduced strength, expansion phenomenon or increased setting time. XRD results showed that the majority of the free lime is hydrated into portlandite from 7 days of hydration (the remaining lime being trapped in dense matrices of portlandite and C-(A)-S-H). The neoformed portlandite is then consumed by the pozzolanic reaction of the calcined clay phases until 180 days of hydration. The presence of free lime does not seem to be problematic in this particular hydrated system. However, its kinetics of hydration and consumption from the pozzolanic reaction can be affected by the cementitious medium when using this calcined material as SCM.

4. Conclusion

This step of study of the hydration of this calcined palygorskite-bearing marlstone highlighted its self-reactivity. The reaction of the calcined clay phases and portlandite (from the hydrated decarbonated dolomite) lead to the formation of C-(A)-S-H, demonstrating the pozzolanic reactivity of this sample. C_2S neoformed during calcination reacts during the first 7 days of hydration. The self-reactivity of this

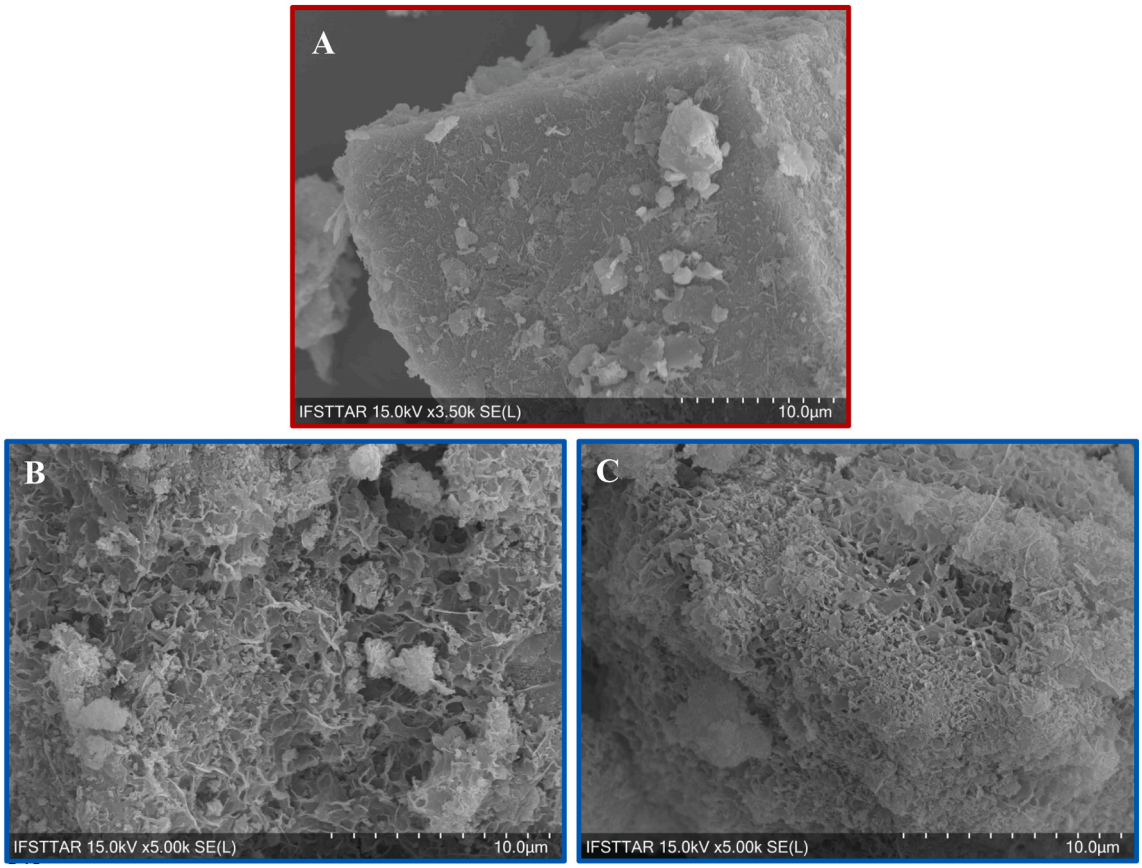

Fig. 5. SEM images of the marlstone calcined at 800 °C (A) and hydrated for 28 days (B and C).

calcined palygorkiste-bearing marlstone is therefore mainly due to its pozzolanic reactivity. The synergy of the phases that compose this sample leads to the consumption of the neoformed portlandite and the incorporation of magnesium from periclase into hydrotalcite and brucite. Now that the reactivity of this calcined material, as well as the evolution of the reactive phases of which it is composed, has been described, the next step will consist of a study of the mechanical and volumetric properties of cementitious blends incorporating this calcined material.

Declaration of Competing Interest

The authors declare that they have no known competing financial interests or personal relationships that could have appeared to influence the work reported in this paper.

Appendix A. Supplementary data

Supplementary data to this article can be found online at https://doi.org/10.1016/j.clay.2021.106372.

References

Almenares, R.S., Vizcaíno, L.M., Damas, S., Mathieu, A., Alujas, A., Martirena, F., 2017. Industrial calcination of kaolinitic clays to make reactive pozzolans. In: Case Studies in Construction Materials, vol. 6, pp. 225–232. https://doi.org/10.1016/j.cscm.2017.03.005.

Alujas, A., Fernández, R., Quintana, R., Scrivener, K.L., Martirena, F., 2015. Pozzolanic reactivity of low grade kaolinitic clays: Influence of calcination temperature and impact of calcination products on OPC hydration. Appl. Clay Sci. 108, 94–101. https://doi.org/10.1016/j.clay.2015.01.028.

Amran, Y.H.M., Alyousef, R., Alabduljabbar, H., El-Zeadani, M., 2020. Clean production and properties of geopolymer concrete; a review. J. Clean. Prod. 251, 119679 https://doi.org/10.1016/j.jclepro.2019.119679.

Andersen, M.D., Jakobsen, H.J., Skibsted, J., 2003. Incorporation of aluminum in the calcium silicate hydrate (C−S−H) of hydrated portland cements: a high-field ^{27}Al and ^{29}Si MAS NMR investigation. Inorg. Chem. 42, 2280–2287. https://doi.org/10.1021/ic020607b.

Andersen, M.D., Jakobsen, H.J., Skibsted, J., 2004. Characterization of white Portland cement hydration and the C-S-H structure in the presence of sodium aluminate by 27Al and 29Si MAS NMR spectroscopy. Cem. Concr. Res. 34, 857–868. https://doi.org/10.1016/j.cemconres.2003.10.009.

Andersen, M.D., Jakobsen, H.J., Skibsted, J., 2006. A new aluminium-hydrate species in hydrated Portland cements characterized by 27Al and 29Si MAS NMR spectroscopy. Cem. Concr. Res. 36, 3–17. https://doi.org/10.1016/j.cemconres.2005.04.010.

Avet, F., Snellings, R., Alujas Diaz, A., Ben Haha, M., Scrivener, K., 2016. Development of a new rapid, relevant and reliable (R3) test method to evaluate the pozzolanic reactivity of calcined kaolinitic clays. Cem. Concr. Res. 85, 1–11. https://doi.org/10.1016/j.cemconres.2016.02.015.

Behim, M., Redjel, B., Jauberthie, R., 2002. Réactivitié du laitier de hauts fourneaux d'Annaba (Algérie) en substitution partielle du ciment.

Bernard, E., Lothenbach, B., Rentsch, D., Pochard, I., Dauzères, A., 2017. Formation of magnesium silicate hydrates (M-S-H). In: Physics and Chemistry of the Earth, Parts A/B/C, Mechanisms and Modelling of Waste-Cement and Cement-Host Rock Interactions, vol. 99, pp. 142–157. https://doi.org/10.1016/j.pce.2017.02.005.

Boudriche, L., Calvet, R., Hamdi, B., Balard, H., 2011. Effect of acid treatment on surface properties evolution of attapulgite clay: an application of inverse gas chromatography. Colloids Surf. A Physicochem. Eng. Asp. 392, 45–54. https://doi.org/10.1016/j.colsurfa.2011.09.031.

Brown, I.W., MacKenzie, K.J.D., Meinhold, R.H., 1987. The Thermal Reactions of Montmorillonite Studied by High-Resolution Solide-State 29Si and 27Al NMR.

Cancio Díaz, Y., Sánchez Berriel, S., Heierli, U., Favier, A.R., Sánchez Machado, I.R., Scrivener, K.L., Martirena Hernández, J.F., Habert, G., 2017. Limestone calcined clay cement as a low-carbon solution to meet expanding cement demand in emerging economies. Dev. Eng. 2, 82–91. https://doi.org/10.1016/j.deveng.2017.06.001.

Cherki El Idrissi, A., Paris, M., Rozière, E., Deneele, D., Darson, S., Loukili, A., 2018. Alkali-activated grouts with incorporated fly ash: from NMR analysis to mechanical properties. Mater. Today Commun. 14, 225–232. https://doi.org/10.1016/j.mtcomm.2018.01.012.

Cherney, E.A., Hooton, R.D., 1987. Cement growth failure mechanism in porcelain suspension insulators. In: IEEE Transactions on Power Delivery, vol. 2, pp. 249–255. https://doi.org/10.1109/TPWRD.1987.4308096.

Cizer, O., Balen, K.V., Gemert, D.V., Elsen, J., n.d. Carbonation and Hydration of Mortars with Calcium Hydroxide and Calcium Silicate Binders 13.

Dai, Z., Tran, T.T., Skibsted, J., 2014. Aluminum INCORPORATION in the C–S–H phase of white Portland cement–metakaolin blends studied by 27Al and 29Si MAS NMR spectroscopy. J. Am. Ceram. Soc. 97, 2662–2671. https://doi.org/10.1111/jace.13006.

Doebelin, N., Kleeberg, R., 2015. *Profex*: a graphical user interface for the Rietveld refinement program *BGMN*. J. Appl. Crystallogr. 48, 1573–1580. https://doi.org/10.1107/S1600576715014685.

El-Diadamony, H., Amer, A.A., Sokkary, T.M., El-Hoseny, S., 2018. Hydration and characteristics of metakaolin pozzolanic cement pastes. HBRC J. 14, 150–158. https://doi.org/10.1016/j.hbrcj.2015.05.005.

Fernandez, R., Martirena, F., Scrivener, K.L., 2011. The origin of the pozzolanic activity of calcined clay minerals: a comparison between kaolinite, illite and montmorillonite. Cem. Concr. Res. 41, 113–122. https://doi.org/10.1016/j.cemconres.2010.09.013.

Florian, P., Veron, E., Green, T.F.G., Yates, J.R., Massiot, D., 2012. Elucidation of the Al/Si ordering in Gehlenite Ca2Al2SiO7 by combined 29Si and 27Al NMR spectroscopy/quantum chemical calculations. Chem. Mater. 24, 4068–4079. https://doi.org/10.1021/cm3016935.

Gao, X., Yu, Q.L., Brouwers, H.J.H., 2017. Apply 29Si, 27Al MAS NMR and selective dissolution in identifying the reaction degree of alkali activated slag-fly ash composites. Ceram. Int. 43, 12408–12419. https://doi.org/10.1016/j.ceramint.2017.06.108.

Garg, N., Skibsted, J., 2014. Thermal activation of a pure montmorillonite clay and its reactivity in cementitious systems. J. Phys. Chem. C 118, 11464–11477. https://doi.org/10.1021/jp502529d.

Garg, N., Skibsted, J., 2016. Pozzolanic reactivity of a calcined interstratified illite/smectite (70/30) clay. Cem. Concr. Res. 79, 101–111. https://doi.org/10.1016/j.cemconres.2015.08.006.

Haha, M.B., Lothenbach, B., Le Saout, G., Winnefeld, F., 2011. Influence of slag chemistry on the hydration of alkali-activated blast-furnace slag — part I: effect of MgO. Cem. Concr. Res. 41, 955–963. https://doi.org/10.1016/j.cemconres.2011.05.002.

Hu, X., Shi, C., Shi, Z., Zhang, L., 2019. Compressive strength, pore structure and chloride transport properties of alkali-activated slag/fly ash mortars. Cem. Concr. Compos. 104, 103392 https://doi.org/10.1016/j.cemconcomp.2019.103392.

Hughes, D.C., Jaglin, D., Kozłowski, R., Mucha, D., 2009. Roman cements — Belite cements calcined at low temperature. Cem. Concr. Res. 39, 77–89. https://doi.org/10.1016/j.cemconres.2008.11.010.

Huntzinger, D.N., Eatmon, T.D., 2009. A life-cycle assessment of Portland cement manufacturing: comparing the traditional process with alternative technologies. J. Clean. Prod. 17, 668–675. https://doi.org/10.1016/j.jclepro.2008.04.007.

Ipavec, A., Gabrovšek, R., Vuk, T., Kaučič, V., Maček, J., Meden, A., 2011. Carboaluminate phases formation during the hydration of calcite-containing portland cement: carboaluminate phase formation. J. Am. Ceram. Soc. 94, 1238–1242. https://doi.org/10.1111/j.1551-2916.2010.04201.x.

Kaminskas, R., Kubiliute, R., Prialgauskaite, B., 2020. Smectite clay waste as an additive for Portland cement. Cem. Concr. Compos. 113, 103710 https://doi.org/10.1016/j.cemconcomp.2020.103710.

Kunhi Mohamed, A., Moutzouri, P., Berruyer, P., Walder, B.J., Siramanont, J., Harris, M., Negroni, M., Galmarini, S.C., Parker, S.C., Scrivener, K.L., Emsley, L., Bowen, P., 2020. The atomic-level structure of cementitious calcium aluminate silicate hydrate. J. Am. Chem. Soc. 142, 11060–11071. https://doi.org/10.1021/jacs.0c02988.

Lippmaa, E., Maegi, M., Samoson, A., Engelhardt, G., Grimmer, A.R., 1980. Structural studies of silicates by solid-state high-resolution silicon-29 NMR. J. Am. Chem. Soc. 102, 4889–4893. https://doi.org/10.1021/ja00535a008.

Magi, M., Lippmaa, E., Samoson, A., Engelhardt, G., Grimmer, A.R., 1984. Solid-state high-resolution silicon-29 chemical shifts in silicates. J. Phys. Chem. 88, 1518–1522. https://doi.org/10.1021/j150652a015.

Massiot, D., Fayon, F., Capron, M., King, I., Le Calvé, S., Alonso, B., Durand, J.-O., Bujoli, B., Gan, Z., Hoatson, G., 2002. Modelling one- and two-dimensional solid-state NMR spectra: Modelling 1D and 2D solid-state NMR spectra. Magn. Reson. Chem. 40, 70–76. https://doi.org/10.1002/mrc.984.

Mikulčić, H., Klemeš, J.J., Vujanović, M., Urbaniec, K., Duić, N., 2016. Reducing greenhouse gasses emissions by fostering the deployment of alternative raw materials and energy sources in the cleaner cement manufacturing process. J. Clean. Prod. 136, 119–132. https://doi.org/10.1016/j.jclepro.2016.04.145. PRES'15: Cleaner energy planning, management and technologies.

Myers, R.J., Bernal, S.A., San Nicolas, R., Provis, J.L., 2013. Generalized structural description of calcium–sodium aluminosilicate hydrate gels: the cross-linked substituted tobermorite model. Langmuir 29, 5294–5306. https://doi.org/10.1021/la4000473.

Pardal, X., Brunet, F., Charpentier, T., Pochard, I., Nonat, A., 2012. 27Al and 29Si solid-state NMR characterization of calcium-aluminosilicate-hydrate. Inorg. Chem. 51, 1827–1836. https://doi.org/10.1021/ic202124x.

Poussardin, V., Paris, M., Tagnit-Hamou, A., Deneele, D., 2020. Potential for calcination of a palygorskite-bearing argillaceous carbonate. Appl. Clay Sci. 198, 105846 https://doi.org/10.1016/j.clay.2020.105846.

Prikhod'ko, R.V., Sychev, M.V., Astrelin, I.M., Erdmann, K., Mangel, A., van Santen, R.A., 2001. Synthesis and Structural Transformations of Hydrotalcite-like Materials Mg-Al and Zn-Al, 74, p. 6.

Richardson, I.G., Groves, G.W., 1993. The incorporation of minor and trace elements into calcium silicate hydrate (C-S-H) gel in hardened cement pastes. Cem. Concr. Res. 23, 131–138. https://doi.org/10.1016/0008-8846(93)90143-W.

Scrivener, K., Martirena, F., Bishnoi, S., Maity, S., 2018. Calcined clay limestone cements (LC3). Cem. Concr. Res. 114, 49–56. https://doi.org/10.1016/j.cemconres.2017.08.017.

Shoval, S., 1988. Mineralogical changes upon heating calcitic and dolomitic marl rocks. Thermochim. Acta 135, 243–252. https://doi.org/10.1016/0040-6031(88)87393-3.

Skibsted, J., Jakobsen, H.J., Hall, C., 1995. Quantification of calcium silicate phases in Portland cements by 29Si MAS NMR spectroscopy. J. Chem. Soc. Faraday Trans. 91, 4423. https://doi.org/10.1039/ft9959104423.

Taylor-Lange, S.C., Rajabali, F., Holsomback, N.A., Riding, K., Juenger, M.C.G., 2014. The effect of zinc oxide additions on the performance of calcined sodium montmorillonite and illite shale supplementary cementitious materials. Cem. Concr. Compos. 53, 127–135. https://doi.org/10.1016/j.cemconcomp.2014.06.008.

Tironi, A., Trezza, M.A., Scian, A.N., Irassar, E.F., 2013. Assessment of pozzolanic activity of different calcined clays. Cem. Concr. Compos. 37, 319–327. https://doi.org/10.1016/j.cemconcomp.2013.01.002.

Van Balen, K., Van Gemert, D., 1994. Modelling lime mortar carbonation. Mater. Struct. 27, 393–398. https://doi.org/10.1007/BF02473442.

Verganelaki, A., Maravelaki, N.-P., Budak, M., n.d. Calcined Clays and Limestone as Hydraulic Binders 9.

Yao, Z.T., Ji, X.S., Sarker, P.K., Tang, J.H., Ge, L.Q., Xia, M.S., Xi, Y.Q., 2015. A comprehensive review on the applications of coal fly ash. Earth Sci. Rev. 141, 105–121. https://doi.org/10.1016/j.earscirev.2014.11.016.

Yazıcı, H., Yardımcı, M.Y., Yiğiter, H., Aydın, S., Türkel, S., 2010. Mechanical properties of reactive powder concrete containing high volumes of ground granulated blast furnace slag. Cem. Concr. Compos. 32, 639–648. https://doi.org/10.1016/j.cemconcomp.2010.07.005.

Zhao, D., Khoshnazar, R., 2020. Microstructure of cement paste incorporating high volume of low-grade metakaolin. Cem. Concr. Compos. 106, 103453 https://doi.org/10.1016/j.cemconcomp.2019.103453.